On the accuracy and limitations of fluid models of the cathode region of dc glow discharges

A Derzsi[1,2], P Hartmann[1], I Korolov[1], J Karácsony[2], G Bánó[1,3] and Z Donkó[1,4]

[1] Research Institute for Solid State Physics and Optics of the Hungarian Academy of Sciences, H-1525 Budapest, POB 49, Hungary
[2] Babeş-Bolyai University, 400084 Cluj-Napoca, M Kogâlniceanu 1, Romania
[3] Department of Biophysics, P J Šafárik University in Košice, 04001 Jesenna 5, Košice, Slovakia

E-mail: donko@mail.kfki.hu

Abstract

This paper compares the performance and limitations of different models of the cathode region of cold-cathode low-pressure dc glow discharges: (i) we review known modelling approaches, (ii) develop our own simulation codes based on these approaches, (iii) perform calculations using these codes for reference sets of discharge conditions, which allows a critical comparison of the models and (iv) for a further check of the simulation results we carry out Langmuir probe measurements of electron densities in abnormal Ar glow discharges. The theoretical approaches include fluid models both neglecting and including the electron energy balance equation, as well as hybrid models, which combine the fluid treatment of slow plasma species with the kinetic simulation of fast electrons. We also test the effect of the choice of the ionization source term in fluid models. We find that the electron densities calculated from the fluid models are far (several orders of magnitude) below the experimental values even if the electron energy equation is considered in the calculations. This weakness of fluid models clearly points out the importance of an accurate calculation of the ionization source term, which can only be accomplished by a kinetic approach under the conditions of highly nonlocal electron transport in the cathode region of glow discharges. In hybrid models Monte Carlo simulation is used for this purpose, and indeed, this approach gives electron densities comparable to our experimental data.

(Some figures in this article are in colour only in the electronic version)

1. Introduction

The precise mathematical characterization of low-temperature discharge plasmas has been motivated both by the advance of applications of discharges and by the wish to understand the rich physics of these systems. The most accurate description can only be expected from calculations based on the kinetic theory, as these plasmas (or at least their certain components, electrons in most cases) are far from equilibrium [1, 2]. In the cathode region of cold-cathode dc glow discharges the electron transport is well known to be highly nonlocal [3, 4] due to the

[4] Author to whom any correspondence should be addressed.

fact that the ionization mean free path of the electrons may be comparable to the spatial extent of the discharge. The exact description of the electrons' motion under such conditions, in principle, may proceed via the solution of the Boltzmann equation. An alternative method of solution is represented by particle methods, which trace 'test' particles to derive the properties of the ensemble of particles. The state of the art for the simulation of electron kinetics in gas discharges based on the numerical solution of the Boltzmann equation has been reviewed in several papers, e.g. [5–7]. While these papers give sophisticated examples, e.g. describe the electron kinetics in the Franck–Hertz experiment, in spatiotemporal relaxation, in

1

J. Phys. D: Appl. Phys. **42** (2009) 225204

A Derzsi *et al*

electromagnetic fields, in inductively and capacitively coupled plasmas, as well as in the positive column of glow discharges, to our best knowledge no full self-consistent solution for the cathode region of plane-parallel dc glow discharges (the simplest possible discharge configuration), where a field reversal occurs in the negative glow [8–10], has been obtained so far by the solution of the Boltzmann equation.

For a self-consistent solution, besides an accurate treatment of the electrons, ions have to be dealt with as well, and the Poisson equation has to be used to calculate the electric field distribution in the presence of appreciable space charge density. For ions the assumption of hydrodynamic (local-field) approximation is reasonable in most dc discharges (operated in a noble gas). In such an approach ions are treated as a continuum.

In fluid models all the plasma species, including electrons, are treated as continuum. Such models are known to be more efficient in terms of computational time, whereas particle-based calculations offer the possibility of a fully kinetic treatment of the particles' motion, going beyond the capabilities of fluid models. The cost of this advantage of particle models is the excessive computation, which, however is a decreasingly serious limitation due to the rapid advance of computer hardware.

The advantages of fluid models (efficiency) and of particle treatment (accuracy) can be jointly utilized in hybrid models [11], in which slow plasma species are treated within the frame of a fluid model, while fast species (in particular fast electrons, which drive ionization and excitation reactions) are treated as particles [12–15]. Although one needs to be aware of their limitations [16], hybrid models have been very successful in describing a wide range of discharge physics phenomena and providing deep insight into the operation of different discharge configurations, such as pseudospark switches [12], analytical glow discharge cells [17] and hollow cathode discharges for gas lasers [18, 19].

One expects that modelling calculations reproduce to certain extent the electrical characteristics of the discharges (which influence to a large extent the energy of ions reaching the cathode) and the density of the charged species (which determine the electric field distribution and the rates of different plasmachemical reactions). Considering low-pressure dc glow discharges in argon, Phelps has compiled a database of electrical characteristics [20]. We are, on the other hand, not aware of any data compilation concerning other characteristics of the same type of discharges, e.g. measured electron density values for a wide range of discharge conditions. The verification of the models present in the literature (cross-checking of the results with experimental data) has been neglected in the majority of works, as no experiments parallel with the modelling studies have been carried out, and due to the fact that there exists no widely available and accepted database for a number of relevant discharge characteristics. It is only the comparison with experimental data that can provide information about the accuracy of any modelling approach and without such comparison statements concerning the performance of the models are questionable.

In spite of their inability to account for kinetic phenomena, fluid models have been attractive for the description of

gas discharge plasmas. They solve a (truncated) set of moment equations of the Boltzmann equation. The first three lowest moments express particle conservation, momentum conservation and energy conservation. Some of the studies published during the last decades consider only particle and momentum balance [21, 22], while the majority of works account for the energy balance as well [23–31]. It is important to recognize that in these works there are significant differences (i) in the choice of boundary conditions of the fluid equations, (ii) in the assumptions concerning the transport coefficients, (iii) in the expression for the ionization source function and (iv) in the choice of the secondary emission coefficient.

The effects of the boundary conditions have recently been discussed by Hagelaar *et al* [32], while issues related to the secondary electron emission coefficient have been addressed in [14, 16, 17, 33, 34] (for low current, Townsend discharges these studies were preceded by [35, 36]).

Unfortunately, most of the papers in the literature present calculations for different sets of discharge conditions and different electrode configurations, thus it is impossible to deduce the effects of assumptions listed above. This could be achieved in the most straightforward way by considering 'standard' sets of discharge conditions (pressure, voltage, electrode separation) and a simple discharge geometry. We will indeed follow this approach in this work: we develop simulation codes based on different types of models, and carry out calculation for common sets of input data. During this study, in particular, our aim is to address the questions:

(i) to what extent is the accuracy of the fluid models improved by incorporating the balance equation for electron energy?

(ii) what is the effect of the form of ionization source function on the calculated discharge characteristics?

(iii) how well fluid modelling calculations approximate experimental results?

To answer these questions we present here fluid modelling calculations both incorporating and disregarding electron energy balance calculation and assuming different forms of the ionization source term. Additional calculations are also executed with a hybrid approach. The basics of these models—based on the literature sources—are reviewed in section 2. Our own calculations are exactly based on these models. For simplicity we carry out our investigations using one-dimensional modelling and we work with argon gas, as for discharges in this gas several independent experimental and modelling results are available, see, e.g. [37] and references therein. Due to the aforementioned lack of reliable experimental data for discharge characteristics, besides the modelling studies we also carry out Langmuir probe measurements of electron temperature and electron density in the negative glow region of argon discharges. The experimental apparatus and the experimental results are described in section 3. Following this, in section 4, we present a critical comparison between the results of calculations based on the different models (which have been described in section 2). Comparison between the simulation results and the experimental data is also given there. Section 5 presents the conclusions of our studies.

2. Modelling approaches

The simulation results, which will be presented in section 4, are based on the models described here. In sections 2.1 and 2.2, respectively, we explain the basics of fluid models *without* energy balance calculation (termed in the following as 'simple fluid models'), as well as of fluid models *with* energy balance calculation (termed as 'extended fluid models'). We discuss the way of self-consistent solution of the models in section 2.3 and the idea of the hybrid approach in section 2.4. The central issue of selecting the transport coefficients in the models is discussed in detail in section 2.5. We also present there a set of transport coefficients (derived from Monte Carlo swarm simulations), which we use in our calculations based on the extended fluid model. Choices for the ionization source term and for the boundary conditions are given in sections 2.6 and 2.7, respectively.

2.1. Simple fluid approach

The simplest fluid models of dc glow discharges (in low-pressure noble gases) include a pair of continuity and a pair of momentum balance equations, for electrons and ions:

$$\frac{\partial n_e}{\partial t} + \frac{\partial \phi_e}{\partial x} = S_e,$$
$$\frac{\partial n_i}{\partial t} + \frac{\partial \phi_i}{\partial x} = S_i, \tag{1}$$

where n_e and n_i are the electron and ion densities, ϕ_e and ϕ_i are the electron and ion fluxes and S_e and S_i are the source functions of electrons and positive ions (see section 2.6). The fluxes are calculated on the basis of the drift–diffusion approximation:

$$\phi_e = -\mu_e n_e E - \frac{\partial (n_e D_e)}{\partial x},$$
$$\phi_i = \mu_i n_i E - \frac{\partial (n_i D_i)}{\partial x}, \tag{2}$$

where E is the electric field, μ_e and μ_i are the mobilities of electrons and ions, respectively. D_e and D_i are the corresponding diffusion coefficients. The assumptions concerning these coefficients will be discussed in section 2.5.

2.2. Extended fluid approach

The nonlocal transport of electrons can to some extent be incorporated into fluid models (see the discussion in [38]) by including an additional equation for the electron mean energy in the set of fluid equations. The energy equation has the form:

$$\frac{\partial n_\varepsilon}{\partial t} + \frac{\partial \phi_\varepsilon}{\partial x} = S_\varepsilon - L_\varepsilon, \tag{3}$$

where $n_\varepsilon = n_e \bar{\varepsilon}$ is the energy density, $\bar{\varepsilon}$ is the mean energy (as a function of position) and ϕ_ε is the energy flux, which can be written as a sum of drift and diffusion terms, similarly to the fluxes of particles, as explained in the paper of Hagelaar and Pitchford [39]:

$$\phi_\varepsilon = -\mu_\varepsilon n_\varepsilon E - \frac{\partial (n_\varepsilon D_\varepsilon)}{\partial x}. \tag{4}$$

The terms in (3):

$$S_\varepsilon(x) = -E(x)\phi_e e \tag{5}$$

and

$$L_\varepsilon(x) = k_L[\bar{\varepsilon}(x)]n_e(x), \tag{6}$$

where k_L is the energy loss rate, represent the gain of energy due to the action of the electric field on electrons and the collisional losses, respectively (e is the elementary charge). μ_ε and D_ε in (4) are the energy mobility and energy diffusion coefficients. Their calculation will be discussed in section 2.5.

2.3. Self-consistent solution

The self-consistent solution of the fluid equations, in the presence of appreciable space charge, characteristic for glow discharges, can be obtained from the Poisson equation:

$$\frac{\partial^2 V}{\partial x^2} = -\frac{e}{\varepsilon_0}(n_i - n_e), \tag{7}$$

where ε_0 is the permittivity of free space.

The set of fluid equations is usually solved using finite difference schemes and with an exponential form of the fluxes [40] due to its stability at spatially changing diffusion/drift conditions [12]. As an alternative to this approach finite element methods are also applicable (see, e.g., [41]).

2.4. Hybrid models

As has already been mentioned in the introduction, the continuum treatment of the ions provides sufficient accuracy in most cases of our interest. This, actually, also holds for the slow electrons that do not contribute to ionization, but does not hold for fast electrons. Hybrid models overcome this problem by treating the fast electrons at the kinetic level (fully capturing their nonlocal character), while retaining the computational efficiency of fluid description of ions and slow electrons. The electron impact contribution to S_i and the source term for slow electrons S_e (which enter the continuity equations of the fluid model) are obtained from a kinetic calculation. Most of the hybrid models apply Monte Carlo (MC) simulation for this purpose.

In the MC procedure the trajectories of fast electrons between successive collisions are followed by direct integration of the equation of motion:

$$m\frac{d^2 r}{dt^2} = q E, \tag{8}$$

where m and $q = -e$ are the mass and the charge of the electron, respectively. The free path between collisions is assigned statistically and the positions of the collisions are calculated from

$$\int_{s_0}^{s_1} N\sigma[\varepsilon(s)]ds = -\ln(1 - R_{01}), \tag{9}$$

where s_0 is the position of the last collision and s_1 is the position of the next collision measured on the curvilinear abscissa s,

J. Phys. D: Appl. Phys. **42** (2009) 225204

A Derzsi *et al*

N is the density of the background gas, σ is the sum of cross sections of all possible elementary processes, ε is the kinetic energy of the particle and R_{01} is a random number with uniform distribution in the $[0, 1)$ interval. Even in one-dimensional models fast electrons are routinely traced in three-dimensional space. Whenever a collision event occurs, the type of collision is chosen on a statistical basis, according to the relative magnitudes of the cross sections of possible processes. In a noble gas, such as Ar, the most important types of collision events include elastic scattering, excitation, as well as ionization. For the details of the simulation of scattering events, see e.g. [42, 43].

The MC module of a hybrid code uses the electric field distribution obtained in the fluid module and provides the source functions of positive ions and slow electrons to be used in the continuity equations of the fluid module. After completing the Monte Carlo simulation cycle of a given number of primary electrons and of the electrons created by them in ionizing collisions, the source functions of ions and slow electrons (in a one-dimensional model) are obtained as

$$S_{i,e}(x) = \frac{j}{e(1 + 1/\gamma)\Delta x} \frac{N_{i,e}(x)}{N_0^{MC}}, \tag{10}$$

where j is the current density calculated in the previous fluid cycle, γ is the electron emission coefficient of the cathode and $N_{i,e}(x)$ is the number of ions (slow electrons) created in the slab of width Δx around x due to the emission of N_0^{MC} primary electrons from the cathode.

The stationary solution of the hybrid model is obtained by iterative solutions of the fluid and Monte Carlo parts. For further details of hybrid models we refer to [12–14].

2.5. Transport coefficients

For the solution of the equations of the fluid models the diffusion and mobility transport coefficients of electrons and ions (and also of the energy density in the case of extended fluid models) have to be specified.

For positive ions a mobility coefficient μ_i that depends on the reduced electric field E/N (N being the gas density), and is known from experiment, is usually included in the fluid and hybrid models. The diffusion coefficient of positive ions is in many cases taken as $D_i/\mu_i = ekT_i$, where k is the Boltzmann constant and kT_i is the characteristic energy of ions. $T_i = T_g$, where T_g is the background gas temperature, is usually assumed (e.g. [12, 21, 28]).

For electrons one can find very different assumptions in the literature. In simple fluid models and in most hybrid models constant values are used for μ_e and D_e. The mobility coefficient usually has an experimental value, and constant characteristic energy values between $kT_e = 0.1$ and $1\,eV$ have routinely been used [44–47] to obtain the diffusion coefficient D_e, via the relation $D_e/\mu_e = ekT_e$. The effect of the assumed value of the (slow, or bulk) characteristic electron energy kT_e has been analysed in [16, 48]. It has been shown that some of the calculated discharge characteristics (particle densities and the depth of the potential well formed in the negative glow) depend sensitively on the assumed value of kT_e, while some

other characteristics (particle fluxes and the voltage–current characteristics of the discharge) are basically independent of this value.

It is trivial that more accurate results could be expected from simple fluid and hybrid models if one could incorporate the dependence of the transport parameters on the discharge conditions. The mobility and diffusion coefficients of electrons are, in fact, known as a function of E/N. Thus one could in principle include the full E/N-dependence of these transport coefficients in a fluid (or hybrid) model. This, however, has been found to result in an instability due to the 'back-diffusion' of electrons into the cathode sheath. For the electrons situated near the sheath–glow boundary the diffusion coefficient increases in the sheath due to the increasing electric field towards the cathode. Consequently, the electrons are able to diffuse against the field, and they reach a region of even higher field, where their diffusion coefficient grows further. This positive feedback is the origin of the instability that one can observe in the simulation. In reality the energy of electrons would quickly decrease when they diffuse against the field, however, the set of fluid equations (1)–(3) cannot account for the electron energy.

The above problem can be overcome by incorporating the electron energy balance equation in fluid models. Nevertheless, even in some of the extended fluid models constant values for μ_e and D_e are sometimes used [23]. Other works use a set of transport coefficients obtained by assuming a Maxwellian electron distribution function (EDF) [29]. The most precise, coherent set of transport coefficients and reaction rates can be obtained from kinetic calculations carried out for electron swarm conditions. This can be accomplished via calculating the EDF either by the solution of the Boltzmann equation [39, 41, 49] or from a Monte Carlo (MC) simulation. The calculations of transport coefficients have to be carried out for a wide range of E/N values and the data obtained this way can subsequently be organized into lookup tables as a function of the mean electron energy. As the energy balance equation in an extended fluid model provides the spatial dependence of the mean energy $\bar\varepsilon$, all the transport coefficients are known, via their dependence on $\bar\varepsilon$, as a function of the space coordinate(s).

Figure 1 illustrates the data generated from our MC swarm simulations which use the cross section set of Hayashi [50] for e^- + Ar collisions. Figure 1(*a*) displays the mobility and diffusion coefficients of electrons (μ_e, D_e) and of the electron energy density (μ_ε, D_ε). To obtain these data we have followed the prescription of the derivation of the particle and energy transport coefficients from the EDF as given in [39]. This set of transport coefficients is used in our simulations based on the extended fluid approach (see section 4).

Finally it is noted that some authors connect the particle and energy transport coefficients via $\mu_\varepsilon = (5/3)\mu_e$ and $D_\varepsilon = (5/3)D_e$, and use a partitioning of the energy (heat) flux $\phi_\varepsilon = (5/3)\phi_e\bar\varepsilon - (5/3)n_e D_e\partial_x\bar\varepsilon$. As has been pointed out in [39], such partitioning that assumes a Maxwellian electron energy distribution, is clearly an approximation.

4
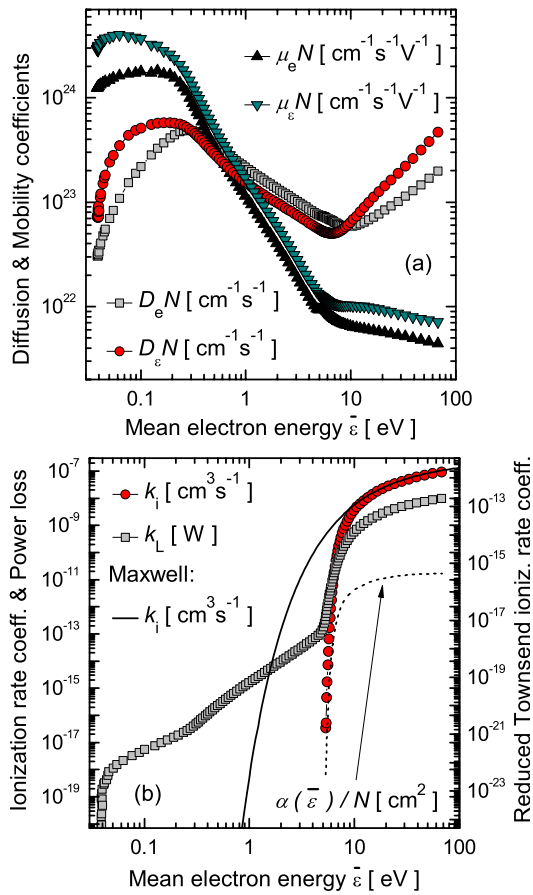
Figure 1. Results of MC swarm simulations. (*a*) Electron and electron energy density transport coefficients as a function of electron mean energy $\bar{\varepsilon}$. (*b*) Ionization rate coefficient (k_i), energy loss rate (k_L) (left scale) and reduced Townsend ionization coefficient $\alpha(\bar{\varepsilon})/N$ (right scale). The solid line in (*b*) showing the ionization rate coefficient assumes a Maxwellian EDF corresponding to the mean electron energy $\bar{\varepsilon}$.

2.6. Source terms

The $S_i(x)$ and $S_e(x)$ source terms in the continuity equations are effective values, i.e. they include both sources and losses of charged particles. The dominant source process in the cathode region is electron impact ionization. Additionally, ionization from metastable levels by electron impact or due to metastable–metastable collisions can also contribute to the sources of electrons and ions. Loss processes, such as recombination, or loss of atomic ions due to their conversion to molecular ions (becoming important at elevated pressures) can be accounted for in the source terms with a negative sign. Here, for simplicity, we consider electron impact ionization of ground state gas atoms as the only source process, and neglect all loss processes.

In the case of fluid models the calculation of the source functions $S(x) = S_i(x) = S_e(x)$ can be based either on the electron flux or the electron density [39]. In simple fluid models the 'flux-based source' calculation uses Townsend's first ionization coefficient α, as a function of the *local* reduced electric field $E(x)/N$:

$$S(x) = \alpha\left[\frac{E(x)}{N}\right]|\phi_e(x)|. \tag{11}$$

In an extended fluid model α as a function of the *electron mean energy* is used and the source function is calculated as

$$S(x) = \alpha[\bar{\varepsilon}(x)]|\phi_e(x)|, \tag{12}$$

The approach based on the electron density uses a rate coefficient k_i, which depends on the electron mean energy:

$$S(x) = k_i[\bar{\varepsilon}(x)]n_e(x)N. \tag{13}$$

This expression will be called the 'rate coefficient-based source' calculation. The accurate approach to obtain the rate coefficient is based on a kinetic calculation of the electron energy distribution function (F_0):

$$k_i(\bar{\varepsilon}) = \sqrt{\frac{2e}{m}} \int_0^\infty \varepsilon\sigma_i(\varepsilon)F_0(\varepsilon)\mathrm{d}\varepsilon, \tag{14}$$

where m is the mass of the electron and σ_i is the ionization cross section. Figure 1(*b*) shows the ionization rate coefficient k_i obtained from our MC swarm simulations, and also the electron energy loss rate k_L to be incorporated in the electron energy balance equation (3) via equation (6). The ionization source function $S(\bar{\varepsilon})$ is also displayed for a Maxwellian energy distribution, as a function of mean energy. In spite of the notable differences, which originate from the non-Maxwellian nature of the EDF for most of the range of $\bar{\varepsilon}$, a Maxwellian EDF has been used in some cases to calculate k_i from the respective cross section [29, 31]. Alternatively, some other authors [23–25] assume an Arrhenius-type behaviour of k_i:

$$k_i = k_{i0}\exp\left(-\frac{E_a}{kT_e}\right), \tag{15}$$

where E_a is the 'activation energy' and k_{i0} is a characteristic parameter of the gas.

As stated by Hagelaar and Pitchford [39], the flux-based calculation of the source function (equation (12)) is expected to be more accurate in the cathode region of glow discharges than the rate coefficient-based calculation, as the accuracy of the calculated electron flux is usually much higher than the accuracy of the calculated density (see, e.g., the findings of [16]). We test in our calculations the source functions given by both forms (12) and (13) in conjunction with (14).

In the hybrid models we use a Monte Carlo simulation of the fast electrons to calculate $S(x)$ for the actual field distribution (as explained in section 2.4).

2.7. Boundary conditions

In our one-dimensional models the discharges are bounded by metallic electrodes. The potentials at the electrodes are fixed as boundary conditions. We use $U(x = 0) = 0\,\mathrm{V}$ at the cathode and $U(x = L) = V$ at the anode, where V is the discharge voltage. The electron and ion densities are taken to be zero at the anode. At the cathode side the gradient of the ion density is taken to be zero, while the electron density is defined by the relation expressing secondary emission:

$$\phi_e(0) = -\gamma\phi_i(0). \tag{16}$$
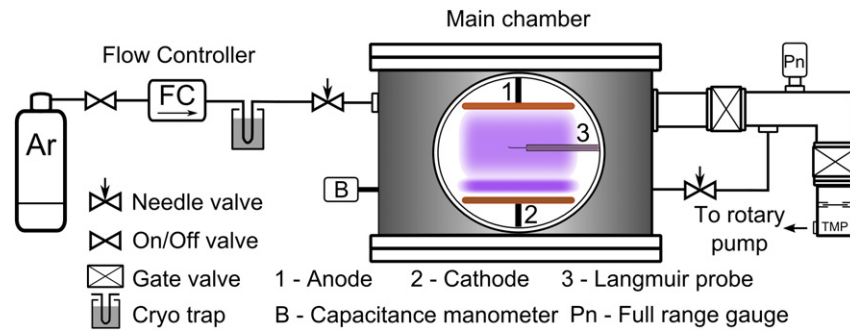
Figure 2. Schematic view of the apparatus.

Here γ is the (apparent) secondary electron emission coefficient. In the strong field near the cathode the fluxes are dominated by the drift contribution, $\phi = nve$, thus the electron density is taken to be $n_e(0) = n_i(0)\mu_i(0)/\mu_e(0)$. The mean electron energy at the cathode side is fixed at $\bar{\varepsilon}(x = 0) = 5\,\mathrm{eV}$, which approximates the average kinetic energy of electrons emitted from the cathode due to ion bombardment. At the anode side $\bar{\varepsilon}$ is taken to be zero at the boundary ($x = L$).

3. Experimental investigations

3.1. Experimental setup

The schematic diagram of the apparatus used in our experiments is shown in figure 2. A dc discharge is generated between two parallel plate electrodes of 7.7 cm diameter. The distance between the cathode and the anode is $L = 3$ cm. The electrodes are made of copper and are placed inside a pyrex glass cylinder to confine the discharge and to prevent long-path breakdown.

A Langmuir probe is situated on the discharge axis 1.5 cm above the cathode. In order to minimize the disturbance of the plasma it is important to keep the dimensions of both the probe and the probe support small. The probe is made of a tungsten wire of $20\,\mu\mathrm{m}$ diameter and has a length of 2.5 mm. The probe support consists of two coaxial glass tubes with the diameter of the outer one being 0.5 mm. The inner glass tube of the probe support is made 1 mm shorter compared with the outer one. This way we can avoid the formation of an electrical contact between the probe surface and the sputtered metal layer deposited onto the support—thus keeping the active probe surface area constant for an extended time period. To prevent the probe surface from being covered by a sputtered metal layer, the probe is regularly cleaned by ion bombardment applying a negative bias voltage of $-120\,\mathrm{V}$ (through a $100\,\mathrm{k}\Omega$ resistor) for a duration of 100 ms. A more detailed description of the Langmuir probe configuration is given in [51].

The discharge tube is placed inside a vacuum chamber. Preceding the measurements, the vacuum part of the apparatus is heated up to 400 K to evaporate volatile impurities from the walls and then pumped down by means of a turbo-molecular pump to a base pressure of $\sim 10^{-5}\,\mathrm{Pa}$. The experiments are conducted using 6.0 purity argon gas with a slow flow of 5–10 sccm, measured and set by a flow controller and a needle valve. Prior to entering the vacuum chamber, the gas is further
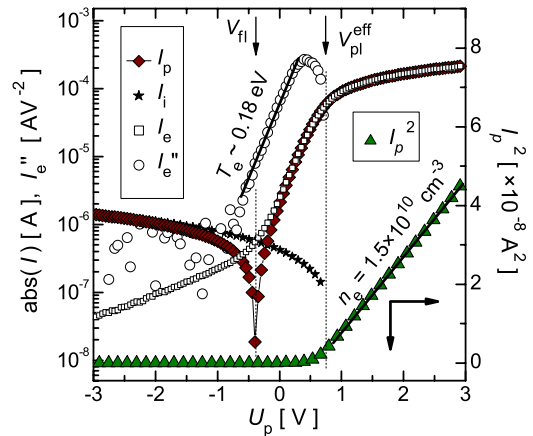
Figure 3. An example of the measured Langmuir probe characteristics $|I_p|$, fit to the ion current I_i, the electron current I_e, second derivative of the electron current I_e'' and the square of the probe current I_p^2 in the argon glow discharge at $p = 40$ Pa and $I = 2$ mA. V_{pl}^{eff} and V_{fl} are the plasma and floating potentials, respectively.

purified in a cold trap filled with liquid nitrogen. Before the measurements, the surface of the cathode is treated by a medium current discharge in argon (≈ 4 mA) for about 15 min.

3.2. Evaluation of the Langmuir probe characteristics

An example of a measured Langmuir probe current–voltage characteristic—for a discharge operating at $p = 40$ Pa and $I = 2$ mA—is shown in figure 3. The absolute value of the probe current $|I_p|$ is plotted on a logarithmic scale as a function of the applied voltage.

Different Langmuir probe evaluation techniques in non-Maxwellian plasmas have been compared in [52]. During the evaluation procedure applied for the present measurements, the second derivative of the total probe current is first calculated (not shown in figure 3). The position of the effective plasma potential V_{pl}^{eff} (which is the plasma potential shifted by the anode-to-probe contact potential) is chosen to be at the zero crossing of the second derivative curve. A preliminary estimate of the electron temperature is obtained by fitting the second derivative with an exponential decay in the electron retardation region close to the plasma potential. Next, the ion part I_i of the probe current is estimated. For the sake of simplicity and because the further evaluation does not rely much on the

J. Phys. D: Appl. Phys. **42** (2009) 225204

A Derzsi *et al*

ion current, in the recent work the ion current is fitted (in the far negative voltage region) by the empirical formula given in [53]: $I_i = I_0[1 - (U - V_{pl}^{eff})/kT_e]^\kappa$. This dependence is then extrapolated to the effective plasma potential. Once the ion current is obtained, the electron current I_e is calculated as $I_e = I_p - I_i$. The near exponential decay of the electron current in the retardation voltage region indicates the presence of a high density of slow electrons in the plasma (see figure 3). Another group of more energetic electrons is responsible for the excessive electron current driven to the probe at even lower voltages. The second derivative of I_e is calculated and fitted by an exponential function to obtain the temperature of the slow electrons.

The square of the probe current I_p^2 is found to exhibit a linear dependence on the probe potential U_p in the electron accelerating region of the characteristic ($U_p > V_{pl}^{eff}$). The electron density is determined from the slope of this line as follows from the orbital motion limited (OML) theory. For detailed description of the Langmuir probe measurements and justification of the applied evaluation methods we refer to [51].

3.3. Experimental results

During the experiments the current–voltage characteristics of the discharge (and the Langmuir probe characteristics) are recorded for discharge current values in the range of $I = 1$–5 mA, at pressures between $p = 13$ and 107 Pa. Our experimental results are shown in figure 4. Panel (*a*) of the figure shows the discharge voltage (V) as a function of the reduced current density (j/p^2) for a series of pL values. Besides our experimental data, those obtained in [54] are also displayed for $L = 3$ cm gap, at $pL = 40$ and 67 Pa cm. Our results compare well with these previous experimental data. Figures 4(*b*) and (*c*), respectively, show the electron density and the (bulk) electron temperature as a function of pressure, recorded at several values of the discharge current. At any fixed pressure the density is nearly proportional to the current. The density measured at the position of the probe exhibits a maximum as a function of pressure (at around 20–25 Pa), this is however a combined effect of the change in the magnitude of the density and the change in the spatial density profile, as a consequence of changing pressure. Nevertheless, as the modelling calculations provide the full spatial distribution of the electron density, the measured data can serve as the basis of comparison, at the point where the probe is located. The electron temperature kT_e has been found to grow both with increasing pressure and with increasing current, acquiring values between 0.1 and 0.35 eV. Our measured data are in good agreement with those ($\sim$0.3 eV) obtained in [55] by Thomson scattering experiment in a discharge cell with plane-parallel electrode configuration. These values correspond to the location of the Ramsauer minimum in the electron–Ar collision cross section.

4. Simulation results and discussion

In this section we present the results of numerical calculations based on the models described in section 2. We perform
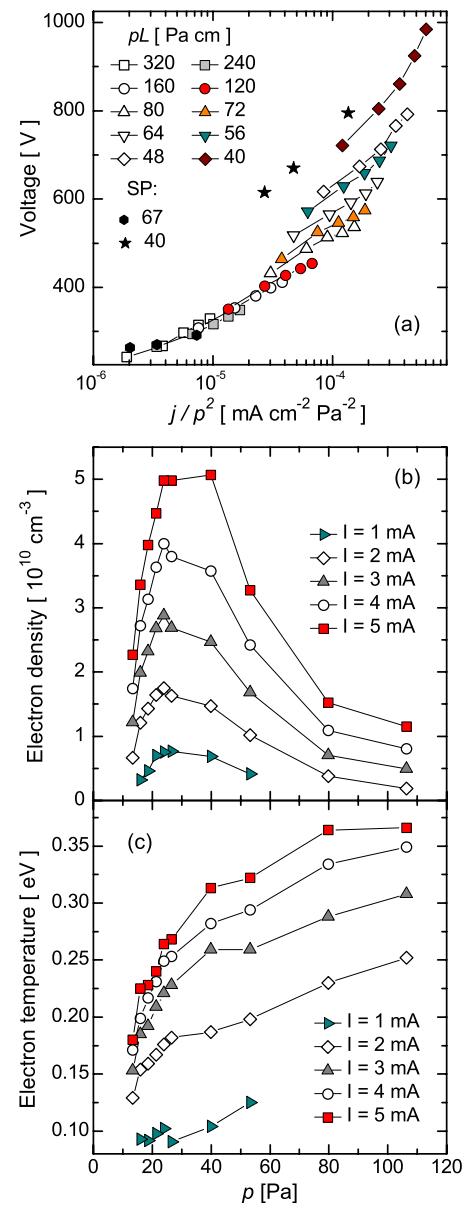
Figure 4. Experimental results: (*a*) discharge voltage as a function of the reduced current density, (*b*) electron density and (*c*) electron temperature as a function of pressure, recorded at fixed values of current. The gas temperature was $T_g \approx 300$ K. 'SP' in (*a*) denotes data from [54].

computations based on both types of fluid approaches: the simple fluid model (without electron energy balance equation) and the extended fluid model (including the electron energy balance equation), as well as based on the hybrid approach, which combines the fluid description of slow electrons and positive ions with the kinetic simulation of fast electrons. The equations and assumptions of each of the models are summarized here again for clarity:

- The *simple fluid model* solves equations (1) and (2) for the number and momentum balance of electrons and ions (see section 2.1) and the Poisson equation (7). The source of ionization is given by the (local-field) flux-based form (11). This model uses an electron mobility $\mu_e p = 3990 \text{ m}^2 \text{ V}^{-1} \text{ s}^{-1}$ Pa [56] and $D_e/\mu_e = ekT_e$,

where the characteristic electron energy kT_e is an input parameter (with values 0.1 and 1.0 eV).

- The *extended fluid model* solves equations (1) and (2) for the number and momentum balance of electrons and ions, equations (3) and (4) for the calculation of the mean electron energy, as well as the Poisson equation (7) for the self-consistency of the solution. For the source of ionization we use both the flux-based form (12) and the rate coefficient-based form (13). The transport coefficients of the electrons and of the electron energy are taken as functions of the mean electron energy from Monte Carlo simulations of electron swarms, see figure 1.

- In the fluid part of the *hybrid model* (applied for positive ions and slow electrons) the continuity and momentum transfer equations (1) and (2) (see section 2.1), and the Poisson equation (7) are solved. For the slow electrons we use the same electron mobility as in the simple fluid model, as well as $D_e/\mu_e = ekT_e$, where the characteristic energy of slow (bulk) electrons kT_e is an input parameter. The source of ionization is calculated by kinetic (Monte Carlo) simulation of fast electrons (see section 2.4).

In each of the models: (i) the mobility of positive ions is taken as a function of E/N [35] and the ion diffusion coefficient is assumed to be $D_i/\mu_i = ekT_i$ with $kT_i = T_g$, as explained in section 2.5; (ii) we assume a homogeneous background gas density (no heating of the gas), (iii) the boundary conditions for the potentials, particle densities and mean electron energy are the ones specified in section 2.7 and (iv) we use a spatial grid of 300 points.

We start here by presenting a cross-check (and validation) of our code (based on the extended fluid approach) with independent modelling results. We have carried out a test simulation for the conditions used by Becker *et al* [41] (the first set of reference conditions): $p = 133$ Pa argon pressure, $T_g = 273$ K temperature, $V = 250$ V voltage, $L = 1$ cm electrode gap, and a secondary emission coefficient of $\gamma = 0.06$. The physical model used in [41] is very similar to ours, except that it also considers the effect of metastable argon atoms. But, as deduced from figure 9(*b*) of that work, ionization processes involving metastable atoms (stepwise ionization, as well as metastable–metastable collisions) contribute a few per cent at most to the overall ion production. A rate-coefficient type source function (13) is used here to match our model with that of [41].

Our code gives results which are in good agreement with those of [41], as revealed in figure 5. The small deviations may be attributed to the use of slightly different transport parameters, as those in [41] have been derived from a somewhat different cross section set [57]. The results presented in this figure also intend to illustrate the capabilities of the extended fluid model. The model is clearly able to reproduce the (ion space charge dominated) sheath + (quasi-neutral) glow structure of the discharge. It predicts a reversal (change in sign) of the electric field [8–10] that occurs due to the highly nonlocal nature of the electron transport in the cathode region. The electron mean energy grows to about 28 eV in the vicinity of the cathode, then decreases in the weaker field further from the cathode and acquires a value of $\bar{\varepsilon} \approx 5\text{–}6$ eV in the
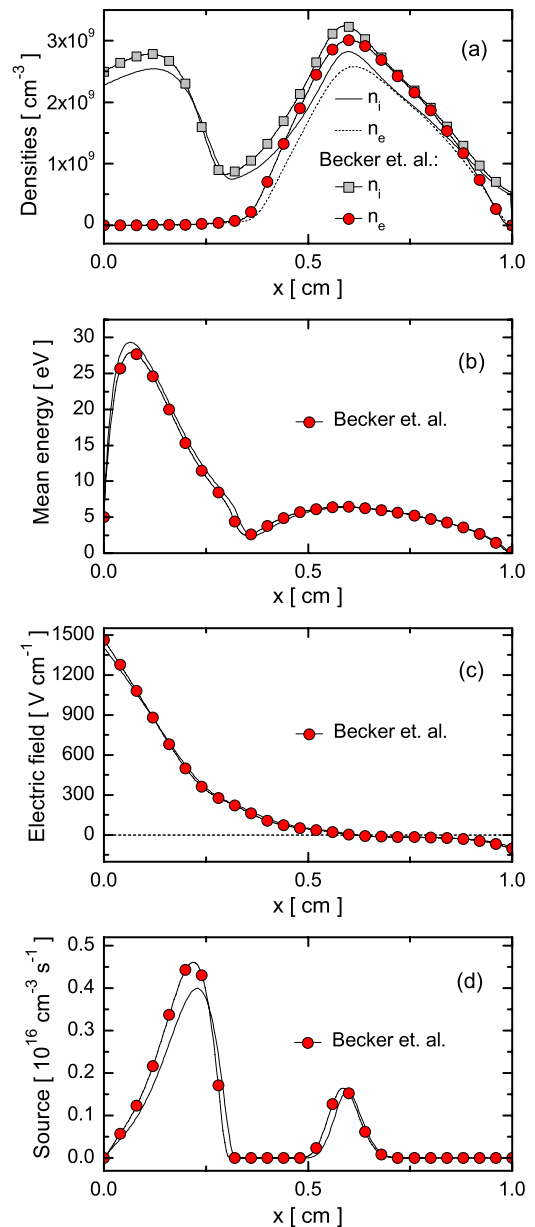
Figure 5. Simulation results for the first set of reference conditions: $p = 133$ Pa, $T = 273$ K, $V = 250$ V, $L = 1$ cm, $\gamma = 0.06$. (*a*) Electron and ion density distributions, (*b*) electron mean energy, (*c*) electric field distribution and (*d*) ionization source function. Solid lines: present data, symbols: data from Becker *et al* [41].

negative glow region. The ionization source is most prominent in the cathode sheath, and it decays around the sheath edge. However, a second peak of ionization also shows up in the negative glow due to the local maxima of the electron density and mean electron energy.

Next, the results of the modelling calculations based on the different types of approaches and using different ionization source terms are compared in figure 6 for the first set of reference conditions: $p = 133$ Pa, $T_g = 273$ K, $V = 250$ V, $L = 1$ cm, $\gamma = 0.06$. The models cover (i) a simple fluid model, (ii) an extended fluid model and (iii) a hybrid model. The source functions in the fluid models are calculated both by the flux-based (equations (11) and (12)) and the rate
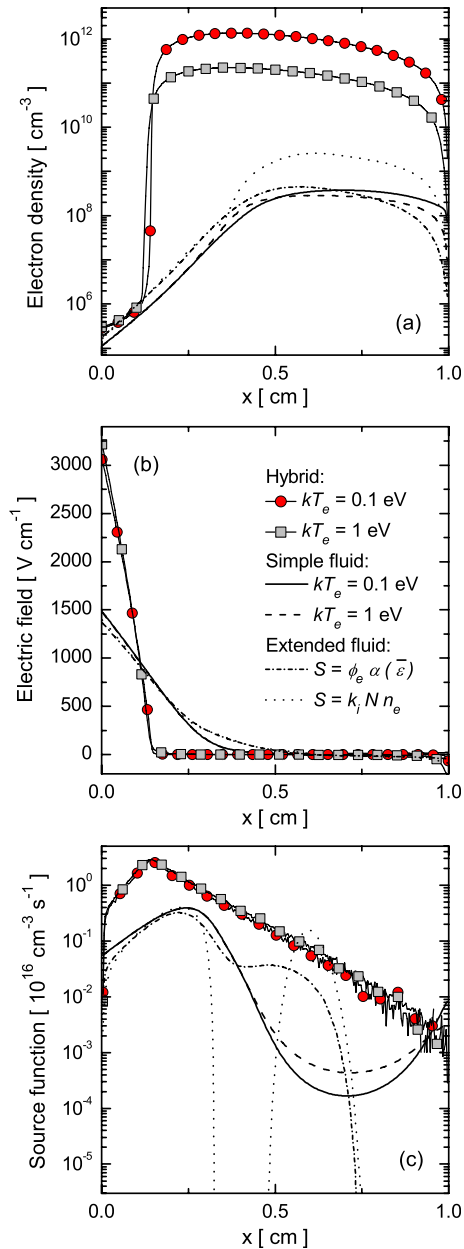
Figure 6. Results obtained by the different modelling approaches for the first set of reference conditions, $p = 133$ Pa, $T_g = 273$ K, $V = 250$ V, $L = 1$ cm, $\gamma = 0.06$. (*a*) Electron density distributions, (*b*) electric field distributions and (*c*) ionization source functions. The legend shown in (*b*) applies to all panels.

coefficient-based (equation (13)) way. In the case of the hybrid model—as explained in section 2.4—the ionization source is obtained from the Monte Carlo simulation of the fast electrons. The simple fluid and hybrid modelling calculations are carried out using both $kT_e = 0.1$ and 1 eV.

Figure 6(*a*) compares the calculated electron density distributions. The peak of the electron density obtained from the different fluid models scatters within one order of magnitude, approximately between 3×10^8–3×10^9 cm^{-3}. Among the fluid models (for this set of discharge conditions) the highest electron density results from the extended approach with the rate coefficient-type ionization source. The hybrid models, in contrast to these values, predict densities in

the range 10^{11}–10^{12} cm^{-3}, depending on the bulk electron temperature assumed.

The electric field distributions resulting from the different models are displayed in figure 6(*b*). The extended fluid model, as well as the hybrid model, predict a reversal of the electric field in the negative glow region. The simple fluid model cannot account for the field reversal, as it does not capture the nonlocal character of electron transport to any extent. The electric field reversal creates a potential well within the negative glow, which supports the accumulation of the electrons. The hybrid model results in a significantly shorter cathode sheath length (and consequently, an approximately factor of two stronger electric field at the cathode), compared with the fluid models.

The ionization source functions calculated by the flux-based approach are compared with the rate coefficient-based ionization source and those obtained from MC simulation in figure 6(*c*). A characteristic feature of the extended fluid model is the source function with two peaks [23, 24, 41], as already seen in figure 5(*d*). When the flux-based calculation of $S(x)$ is used, the double-peaked structure disappears.

It is only the hybrid model (which traces the fast electrons by Monte Carlo simulation) that produces an exponential fall-off of the ionization source term past the sheath-glow boundary. As the ionization and excitation cross sections have similar forms and both processes are primarily driven by fast electrons (of which the energy may exceed by far the thresholds of these processes), it is reasonable to assume that the spatial distribution of the excitation rate exhibits the same behaviour as the ionization. This has indeed been confirmed for the case of the cathode region of dc glow discharges [58]. The light intensity in the negative glow is known to decrease exponentially, see e.g. [47, 59], and such behaviour is predicted by the hybrid model only. Predictions of the fluid models are in sharp contrast to this. The different models also result in different values for current density: the simple fluid model gives 0.14 mA cm^{-2}, the extended fluid model with the rate coefficient and flux-based calculation of the ionization source, respectively, gives 0.125 and 0.12 mA cm^{-2}. For the same conditions, the hybrid model (with $kT_e = 1$ eV) gives 0.825 mA cm^{-2}.

At this point we can already conclude that there are significant differences in the predicted discharge characteristics as obtained from the different models. It is only the comparison with experimental data that can help find the best approach and provide information about the reliability of the models. Thus, next we take another set of reference conditions for which the electrical characteristics, as well as electron density and electron temperature data, have been measured in our experiment. The detailed comparison of the spatial distribution of the electron density, electric field and ionization source function is presented in figure 7 for the second set of reference conditions: $p = 40$ Pa, $V = 441$ V (corresponding to a measured current of 4 mA), $T_g = 300$ K, $L = 3$ cm, $\gamma = 0.033$. This value of the secondary yield (being in agreement with results given in [58]) was chosen in a way that the current calculated by the hybrid model matches the experimental value.
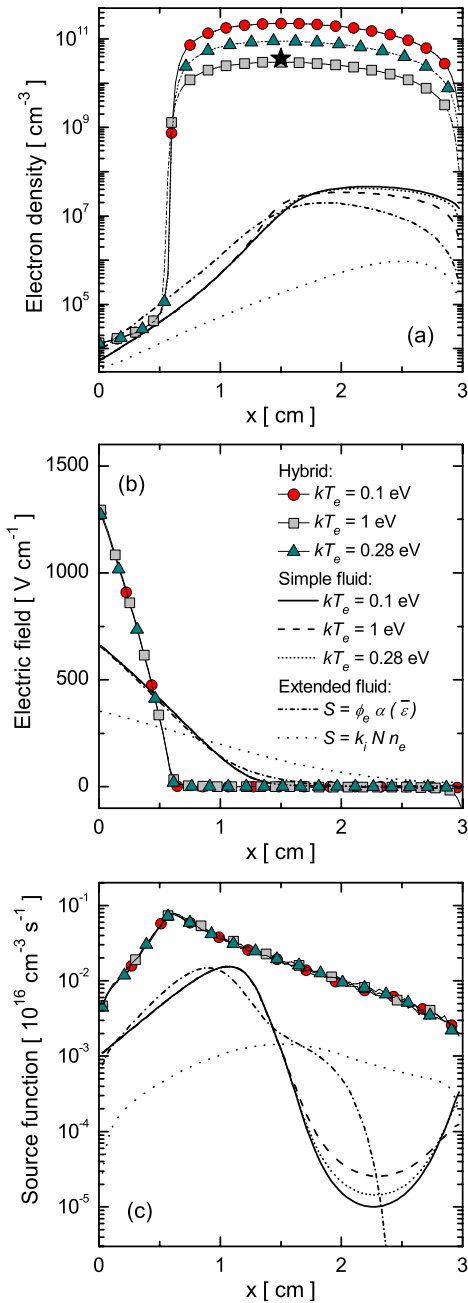
Figure 7. Results obtained by the different modelling approaches for the second set of reference conditions, $p = 40$ Pa, $V = 441$ V, $T_g = 300$ K, $L = 3$ cm, $\gamma = 0.033$. (*a*) Electron density distributions, (*b*) electric field distributions and (*c*) ionization source functions. The symbol ★ in (*a*) shows the density determined by the Langmuir probe measurement. The legend shown in (*b*) applies to all panels.

The behaviour of the quantities analysed here is very similar to their behaviour shown in figure 6 for the first set of reference conditions. In addition to the bulk electron temperature values $kT_e = 0.1$ and 1 eV, used previously, figure 7 also shows the results of simple fluid and hybrid modelling calculations using a value $kT_e = 0.28$ eV determined experimentally for this set of discharge conditions. The hybrid simulation with this value of kT_e results in an electron density within a factor of two agreement with the
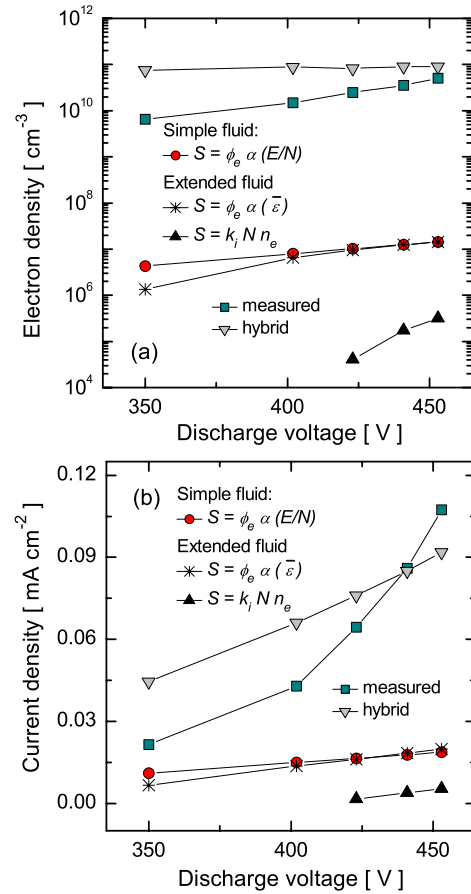
Figure 8. Electron density at $x = 1.5$ cm from the cathode (*a*) and current density (*b*), as a function of discharge voltage at $p = 40$ Pa pressure. $\gamma = 0.033$ was used in all calculations.

experimentally determined n_e, as shown in figure 7(*a*). All the fluid calculations give about three orders of magnitude lower density. The extended fluid model with the rate coefficient-based source gives the lowest density and does not even predict the formation of a fully-developed sheath + glow structure for these conditions, as seen in figure 7(*b*). The source functions (see figure 7(*c*)) exhibit complex shapes, in contrast to those resulting from the hybrid model (which indicates exponential fall-off beyond the sheath–glow boundary).

Finally, we examine how the experimentally observed changes in the electron density and electrical characteristics are reproduced by the models. Figure 8 shows the electron density at the position of the Langmuir probe ($x = 1.5$ cm) and the discharge current density as a function of the discharge voltage. Besides the experimental data the figure displays the results of the hybrid model and the different fluid models (simple fluid model, as well as extended fluid models with flux-based and rate coefficient-based calculation of the ionization source term). Concerning the electron density (figure 8(*a*)), among all the models the hybrid approach gives results which are closest to the experimental values. Differences are attributed to (i) the possible underestimation of the electron density by the very presence of the probe itself in the plasma and (ii) the overestimation of the density by the models due to the fact that—being one-dimensional—they do not consider radial losses of charged particles. The experimental data

show a factor of five change in the electron density within the current range studied ($1\,\text{mA} \leqslant I \leqslant 5\,\text{mA}$). The hybrid calculations, carried out with the measured values of kT_e and a constant secondary yield $\gamma = 0.033$ predict a nearly constant density. Improved estimates for n_e would be expected with a hybrid model using a calculated γ based on the kinetic simulation of heavy particles [14, 45]. The fluid models give a slowly increasing density with increasing voltage, but the magnitudes of the n_e ($x = 1.5\,\text{cm}$) values, particularly the ones derived from the extended fluid model with a rate coefficient-based calculation of the source term, are far ($\sim$3–5 orders of magnitude) below the measured values.

The measured and calculated current densities are shown in figure 8(*b*). The fluid models result in a slight positive slope of the curves with current density values lying well below the experimental data, especially at higher voltages. In particular, the current densities given by the extended fluid model with the rate coefficient-based calculation of the source term gives more than an order of magnitude lower values than the measured data. The hybrid model with a constant secondary yield predicts the discharge current within approximately a factor of two, for the whole range of interest.

5. Conclusions

This paper intended to critically compare different modelling approaches applicable for the description of the cathode region of low-pressure dc glow discharges. We have considered simple and extended fluid models, which, respectively, neglect and include the balance equation for electron energy (the third moment of the electron Boltzmann equation). In the simple fluid model we used constant mobility and diffusion coefficients for electrons and E/N-dependent transport coefficients for positive ions. We have found that using E/N-dependent electron transport coefficients in a simple fluid model results in a 'back-diffusion' of electrons into the sheath. The extended fluid models avoid this problem by using electron transport coefficients, which depend on the local electron mean energy rather than on the local reduced electric field. The spatial distribution of the electron mean energy is derived from the third moment equation of the Boltzmann equation. The transport coefficients of the electron energy together with the transport coefficients of the electrons have been determined from Monte Carlo simulations of electron swarms for a wide range of E/N values.

We have also tested the effect of the choice of the ionization source term, covering the flux-based and rate coefficient-based calculations of $S(x)$, as well as its direct determination from Monte Carlo simulation for the actual field distribution in the cathode region.

Our conclusions regarding the accuracy of fluid models for the description of the cathode region of dc glow discharges are not favourable. The electron densities obtained from the different models have scattered over several orders of magnitude, the best agreement with experimental data has been found using the hybrid model. While reproducing the basic discharge physics of the cathode region, the different fluid

approaches, depending on the form of the ionization source term, underestimated the electron density in the negative glow by three or more orders of magnitude. Thus we conclude that far more accurate results can be obtained from hybrid models than from fluid models, especially if the temperature of bulk electrons—which is needed as input in the simulation—can be determined experimentally. The hybrid approach has also been found superior over fluid models in predicting the electrical characteristics of the discharges and the spatial distribution of processes driven by highly energetic electrons.

We believe that the large discrepancies between the results of the fluid and hybrid calculations originate from the highly nonlocal nature of electron transport in the cathode region, which even by the extended fluid modelling can be captured only to a very limited extent. Here a kinetic approach, such as Monte Carlo simulation, to describe electron kinetics has a clear and indispensable advantage over the fluid treatment. The improvements of the accuracy of fluid models by incorporating the electron energy balance equation (compared with those which neglect it) have proven to be marginal. Thus, predictions of fluid models of the cathode region of glow discharges have to be treated with reservations.

Acknowledgments

References

[1] Robson R E, White R D and Petrović Z Lj 2005 *Rev. Mod. Phys.* **77** 1303
[2] Pitchford L C, Boeuf J-P, Segur P and Marode E 1990 *Non-equilibrium Effects in Ion and Electron Transport* ed J W Gallagher (New York: Plenum)
[3] Tsendin L D 1995 *Plasma Sources Sci. Technol.* **4** 200 Tsendin L D 2009 *Plasma Sources Sci. Technol.* **18** 014020
[4] Kudryavtsev A A, Morin A V and Tsendin L D 2008 *Tech. Phys.* **53** 1029
[5] Winkler R, Arndt S, Loffhagen D, Sigeneger F and Uhrlandt D 2004 *Contrib. Plasma Phys.* **44** 437
[6] Kolobov V I and Arslanbekov R R 2006 *IEEE Trans. Plasma Sci.* **34** 895
[7] Petrović Z Lj, Raspopović Z M, Dujko S and Makabe T 2002 *Appl. Surf. Sci.* **192** 1
[8] Boeuf J-P and Pitchford L C 1995 *J. Phys. D: Appl. Phys.* **28** 2083
[9] Pinheiro M 2004 *Phys. Rev.* E **70** 056409
[10] Kudryavtsev A A and Toinova N E 2005 *Tech. Phys. Lett.* **31** 370
[11] Surendra M, Graves D B and Jellum G M 1990 *Phys. Rev.* A **41** 1112
[12] Boeuf J-P and Pitchford L C 1991 *IEEE Trans. Plasma Sci.* **19** 286

J. Phys. D: Appl. Phys. **42** (2009) 225204

A Derzsi *et al*

[13] Bogaerts A, Gijbels R and Goedheer W J 1996 *Anal. Chem.* **68** 2296
[14] Donkó Z 2001 *Phys. Rev.* E **64** 026401
[15] Brok W J M, Wagenaars E, van Dijk J and van der Mullen J J A 2007 *IEEE Trans. Plasma Sci.* **35** 1325
[16] Donkó Z, Hartmann P and Kutasi K 2006 *Plasma Sources Sci. Technol.* **15** 178
[17] Bogaerts A and Gijbels R 2002 *Plasma Sources Sci. Technol.* **11** 27
[18] Bánó G, Szalai L, Horváth P, Kutasi K, Donkó Z, Rózsa K and Adamowicz T M 2002 *J. Appl. Phys.* **92** 6372
[19] Bogaerts A and Grozeva M 2003 *Appl. Phys.* B **76** 299
[20] Phelps A V http://jilawww.colorado.edu/~avp/collision_data/cathodefalldata/arcathiv.txt
[21] Kim H C, Hur M S, Yang S S, Shin S W and Lee J K 2002 *J. Appl. Phys.* **91** 9513
[22] Kim H J, Kwon D C and Yoon N S 2007 *J. Korean Phys. Soc.* **51** 633
[23] Graves D B and Jensen K F 1986 *IEEE Trans. Plasma Sci.* **14** 78
[24] Meyyappan M and Kreskovsky J P 1990 *J. Appl. Phys.* **68** 1506
[25] Lin Y H and Adomaitis R A 1998 *Phys. Lett.* A **243** 142
[26] Qin W, Cohen I M and Ayyaswamy P S 2000 *Phys. Plasmas* **7** 719
[27] Brok W J M, van Dijk J, Bowden M D, van der Mullen J J A M and Kroesen G W M 2003 *J. Phys. D: Appl. Phys.* **36** 1967
[28] Elaissi S, Yousfi M, Charrada K and Troudi L 2005 *Eur. Phys. J. Appl. Phys.* **32** 37
[29] Costin C, Marques L, Popa G and Gousset G 2005 *Plasma Sources Sci. Technol.* **14** 168
[30] Kothnur P S and Raja L L 2005 *J. Appl. Phys.* **97** 043305
[31] Wang Q, Economou D J and Donnelly M 2006 *J. Appl. Phys.* **100** 023301
[32] Hagelaar G J M, de Hoog F J and Kroesen G M W 2000 *Phys. Rev.* E **62** 1452
[33] Bokhan A P, Bokhan P A and Zakrevsky D E 2005 *Appl. Phys. Lett.* **86** 151503
[34] Bokhan A P, Bokhan P A and Zakrevsky D E 2005 *Tech. Phys.* **50** 1233
[35] Phelps A V and Petrović Z Lj 1999 *Plasma Sources Sci. Technol.* **8** R21
[36] Phelps A V, Pitchford L C, Pedoussat C C and Donkó Z 1999 *Plasma Sources Sci. Technol.* **8** B1
[37] Phelps A V 2001 *Plasma Sources Sci. Technol.* **10** 329
[38] Kim H C, Iza F, Yang S S, Radmilović-Radjenović M and Lee J K 2005 *J. Phys. D: Appl. Phys.* **38** R283
[39] Hagelaar G J M and Pitchford L 2005 *Plasma Sources Sci. Technol.* **14** 722
[40] Sharfetter D L and Gummel H K 1969 *IEEE Trans. Electron Devices* **ED-16** 64
[41] Becker M M, Loffhagen D and Schmidt W 2009 *Comput. Phys. Commun.* **180** 230
[42] Bogaerts A, van Straaten M and Gijbels R 1995 *Spectrochim. Acta* B **50** 179
[43] Kutasi K and Donkó Z 2000 *J. Phys. D: Appl. Phys.* **33** 1081
[44] Bogaerts A, Gijbels R and Goedheer W J 1995 *J. Appl. Phys.* **78** 2233
[45] Donkó Z 2000 *J. Appl. Phys.* **88** 2226
[46] Revel I, Pitchford L C and Boeuf J-P 2000 *J. Appl. Phys.* **88** 2234
[47] Marić D, Kutasi K, Malović G, Donkó Z and Petrović Z Lj 2002 *Eur. Phys. J.* D **21** 73
[48] Kutasi K, Hartmann P, Bánó G and Donkó Z 2005 *Plasma Sources Sci. Technol.* **14** S1
[49] Arslanbekov R R and Kolobov V I 2003 *J. Phys. D: Appl. Phys.* **36** 2986
[50] Hayashi M 2003 Bibliography of electron and photon cross sections with atoms and molecules published in the 20th century—argon *Report No.* NIFS-DATA-72 National Institute For Fusion Science
[51] Bánó G, Hartmann P, Kutasi K, Horváth P, Plasil R, Hlavenka P, Glosik J and Donkó Z 2007 *Plasma Sources Sci. Technol.* **16** 492
[52] Godyak V A, Piejak R B and Alexandrovich B M 1993 *J. Appl. Phys.* **73** 3657
[53] Nuhn B and Peter G 1977 *Proc. 13th Int. Conf. on Phenomena. Ionized Gases (Berlin)* p 97 (contributed papers)
[54] Stefanović I and Petrović Z Lj 1997 *Japan. J. Appl. Phys.* **36** 4728
[55] Gamez G, Bogaerts A, Andrade F and Hieftje G M 2004 *Spectrochim. Acta* B **59** 435
[56] Ward A L 1962 *J. Appl. Phys.* **33** 2789
[57] Loffhagen D personal communication
[58] Marić D, Hartmann P, Malović G, Donkó Z and Petrović Z Lj 2003 *J. Phys. D: Appl. Phys.* **36** 2639
[59] Rózsa K, Gallagher A and Donkó Z 1995 *Phys. Rev.* E **52** 913